GEOPHYSICAL RESEARCH LETTERS, VOL. ???, XXXX, DOI:10.1029/,

Origins of Simulated Decadal Variability in the Southern Ocean Region

X. Qu

Department of Atmospheric and Oceanic Sciences, University of California,
Los Angeles, PO BOX 951565, CA 90095-1565

J. Boé

Department of Atmospheric and Oceanic Sciences, University of California,
Los Angeles, PO BOX 951565, CA 90095-1565

A. Hall

Department of Atmospheric and Oceanic Sciences, University of California,
Los Angeles, PO BOX 951565, CA 90095-1565

X. Qu, Department of Atmospheric and Oceanic Sciences, University of California, Los Angeles, PO BOX 951565, CA 90095-1565, USA. (xinqu@atmos.ucla.edu)

Pre-industrial control experiments of 15 climate models are used to examine decadal variability in the surface climate of Southern Hemisphere extratropics. We find the climate over the Southern Ocean exhibits large decadal variability in all simulations, underscoring the distinctiveness of this region's internal variability. In every model, decadal variations in surface temperature and sea-ice are closely linked, possibly due to sea-ice albedo feedback. These similarities aside, we find there is two- to three-fold intermodel spread in the magnitude of the decadal variability. We apply linear stochastic theory to 'model the models', and find that it almost perfectly captures the models' behavior. This exercise also reveals that most of the intermodel spread in decadal variability can be attributed to differences in climate feedbacks.

1. Introduction

While there has been a large-scale decrease in total Arctic sea-ice cover over the past three decades [Cavalieri et al., 1997; Rothrock et al., 1999; Vinnikov et al., 1999; Serreze et al., 2003; Stroeve et al., 2008; Parkinson and Cavalieri, 2008], comparable trends are not evident around Antarctica [Cavalieri et al., 1997; Vaughan et al., 2003; Cavalieri and Parkinson, 2008]. This large-scale stability, however, masks substantial regional trends with opposing signs. For instance, over the past few decades, sea-ice has been advancing in the western Ross Sea, and retreating adjacent to the western Antarctic Peninsula and southern Bellingshausen Sea region [Liu et al., 2003; Cavalieri and Parkinson, 2008]. The origin of these regional trends and associated temperature anomalies, whether internally-generated by the climate system or anthropogenic, is still largely unknown. Determining the cause of the trends is complicated by the fact that the climate system may generate larger decadal variability in the Southern Ocean than other regions. This excess internal variability may result from climate processes unique to the Southern Ocean [e.g., Fig. 1; Manabe and Stouffer, 1996]. To assess whether the observed trends arise at least in part from greenhouse warming, a better understanding of these processes and their role in internal decadal variability is necessary.

Unfortunately, observations of sufficient duration to analyze decadal variability are extremely sparse in the Southern Ocean. An alternative approach is to examine decadal variability in models. Here, we examine internal decadal variability over the Southern Ocean in “pre-industrial control experiments” from 15 climate models used in the Fourth Assessment Report (AR4) of the Intergovernmental Panel of Climate Change. As we show in Fig. 1, the simulations all exhibit large decadal variability over the Southern Ocean, possibly lending credence to the idea that recent trends may be internally-generated. However, there is also a twofold difference in the magnitude of the variability across models, greatly complicating efforts to assess origins of recent trends quantitatively. Here we examine why the models differ so much in their overall levels of decadal variability.

There are many possible reasons for the intermodel spread, including differences in (1) energy levels of atmospheric eddies, which presumably play a central role in forcing climate variability on all time scales [Hasselmann, 1976], (2) attenuating and amplifying effects of climate feedbacks on decadal temperature anomalies [North et al., 1981], and (3) heat exchange associated with the ocean circulation, which sets the climate system's effective heat capacity [North et al., 1981; Hall and Manabe, 1997]. To understand the role of these factors, following North et al. [1981], we apply linear stochastic theory to an energy balance equation.

$$C\frac{\partial T'}{\partial t} = -\lambda T' + \eta' \tag{1}$$

where T' represents variations in SAT. In the energy balance framework, SAT represents the thermodynamic response of the coupled atmosphere/ocean mixed layer system. The first term on the right side of Eq. (1) represents damping processes of T', with their effectiveness determined by a linear coefficient, λ. Values of λ are in turn modulated by climate feedbacks. A prominent climate feedback over the Southern Ocean is sea-ice albedo feedback. It tends to amplify T' by modulating net incoming solar radiation [e.g., Hall, 2004]. Stronger sea-ice albedo feedback thus results in smaller λ. The second term on the right side represents atmospheric white-noise forcing (AWNF), which encapsulates the climatic impacts of short-term near-surface heat and wind fluctuations associated with atmospheric eddies. These two terms together determine thermal variations of the system, represented by the term on the left side of Eq. (1). C on the left side is an effective heat capacity of the system. Given the two terms on the right side, larger C implies slower response of T'. Since the heat capacity of air is much smaller than water, C is largely determined by the effective depth of the ocean mixed layer, or alternatively, the effective vertical penetration of surface temperature variations in the Southern Ocean.

In spite of its simplicity, this framework is remarkably accurate in predicting overall levels of simulated variability over the Southern Ocean. Thus it is a useful "model of the models", and allows us to ascertain in broad terms what is causing the models to disagree.

2. Data Sets

Simulated climate is examined in "pre-industrial control experiments" with 15 AR4 models (see Table 1), archived at Lawrence Livermore National Laboratory (http://www-pcmdi.llnl.gov/). In these experiments, climate forcings such as greenhouse gas and aerosol concentrations are fixed at pre-industrial levels. Although pre-industrial control simulations are available for 23 AR4 models, only the 15 models listed in Table 1 provide long enough time series to calculate stable climate statistics in the Southern Ocean. (The length of time series differs from model to model, and ranges from 330 to 500 years.) The 15 models all have somewhat different horizontal resolutions. To ensure we examine variability on similar spatial scales, all data are interpolated onto a common coarse-resolution grid prior to any calculations. We use annual-mean quantities for all the analyses. Decadal variability is defined as all variability with time scales longer than 10 years after the long-term linear trends of data are removed. In this study, the main climate variable of interest is SAT because of its role in Eq. (1). However, we also show some sea-ice concentration variability results both because of the broader interest in this variable and to demonstrate its clear connection to SAT variability.

3. Climate Variability in the Southern Ocean Region

Annual-mean SH extratropical SAT exhibits enhanced variability south of 50^0S in all simulations (Fig. 1A). The variability tends to peak near 68^0S, where the ensemble-mean of zonal-mean standard deviation (SD) of SAT reaches about 1K. This is also the place where the largest interannual variability in annual-mean SIC occurs (Fig. 1B). Decadal variability of SAT and SIC has a similar zonal distribution to that of interannual SAT and SIC variability (Fig. 1C and D). First, there is significantly more variability south of 50^0S in all simulations and second, the ensemble-mean SDs of decadal SAT and SIC peak near 68^0S. Comparison with Figs.1A and B suggests about 40% of SAT and SIC variance is decadal.

Despite the fact that Southern Ocean SAT and SIC decadal variability is elevated in all models, the magnitude of the variability varies significantly from model to model. SD of decadal SAT at the peak latitude ranges from 0.3 to 0.9K, and that of decadal SIC ranges from about 2.4% to 6.9%, both corresponding to a threefold intermodel spread. To measure intermodel spread in the variability of the Southern Ocean as a whole, we average SDs of decadal SAT and SIC over the Southern Ocean. As shown in Table 1, regional-mean decadal SAT SD ranges from 0.25 to 0.61K, and regional-mean decadal

SIC SD ranges from 2.19 to 4.07%, both corresponding to about a twofold intermodel spead.

As is clear from both Fig. 1 and Table 1, SAT and SIC decadal variations are closely linked. First, magnitudes of the variability in both quantities peak near 68^0S. This latitude signifies the location of zonal-mean annual-mean sea-ice edge. Second, overall levels of variability of the two quantities are strongly correlated across models (the correlation coefficient is 0.73), indicating models with greater decadal variability in SAT tend to have greater decadal variability in SIC as well. This association is probably largely due to sea-ice albedo feedback, whose effects on T' are implicit in λ.

4. Factors Controlling Decadal Variability

From Eq. (1), we derive a spectrum of T':

$$|\tilde{T}'(\omega)|^2 = \frac{|\tilde{\eta}|^2/C^2}{1 + a^2 - 2acos(2\pi\omega)} \qquad (2)$$

The term on the left side of Eq. (2) represents the power spectral density of SAT, given in terms of the lag-one year autocorrelation coefficient of T', a, power spectral density of AWNF, $|\tilde{\eta}|^2$, effective heat capacity, C, and angular frequency, ω. The term a quantifies the persistence of T' from year to year, and is related to λ and C through $a = 1 - \triangle t \cdot (\lambda/C)$, where $\triangle t$ represents the sampling interval of data, which is 1 year [e.g., Lemke et al., 1980].

To validate this framework and use it to shed light on differences in modeled Southern Ocean variability, first we calculate Southern Ocean regional-mean values of a. As shown in Table 1, the intermodel range in a is from 0.13 to 0.65, representing a fivefold intermodel spread. While many models have a very red spectrum in the Southern Ocean, others exhibit almost no persistence from year to year. Since a is determined by both λ and C, this may be an indication of large intermodel differences in either climate feedbacks or the effective heat capacity of the system or both. Then, we calculate the Southern Ocean regional values of $|\tilde{\eta}|^2/C^2$ by integrating Eq. (2) over all frequencies resolved by the data,

$$\int |\tilde{T'}(\omega)|^2 d\omega = |\tilde{\eta}|^2/C^2 \int \frac{1}{1+a^2-2acos(2\pi\omega)} d\omega \tag{3}$$

The integral on the left-hand side of Eq. (3) represents SAT variance, whose square roots are shown in Table 1. Given the Southern Ocean regional-mean values of a, the integral on the right-hand side of Eq. (3) can be evaluated. Then values of $|\tilde{\eta}|/C$ can be obtained from Eq. (3). As shown in Table 1, the intermodel range in $|\tilde{\eta}|/C$ is from 0.62 to 1.18Kyear$^{1/2}$, with 2/3 of the models in the 0.8-1.0Kyear$^{1/2}$ range. Though not negligible, these intermodel differences are much smaller than those in values of a.

Once we know values of a and $|\tilde{\eta}|/C$, we can obtain an expression for decadal variance of T' by integrating Eq. (2) over frequencies lower than 1 cycle per decade. Here we assume $|\tilde{T'}(\omega)|^2$ is a constant function of frequency for time scales longer than 10 years. This assumption is valid if the characteristic time scale of the Southern Ocean is much shorter than 10 years. The characteristic time scale, represented by C/λ, can be calculated with the expression $a = 1 - \triangle t \cdot (\lambda/C)$ [e.g., Hall and Manabe, 1997]. It ranges from 1.1 to 2.9 years, indeed shorter than 10 years. Therefore our assumption is justified, and we obtain a simple expression for SD of decadal T':

$$SD \propto \frac{|\tilde{\eta}|/C}{1-a} \tag{4}$$

Larger values of both a and $|\tilde{\eta}|/C$ lead to greater levels of decadal variability. To assess whether Eq. (4) accurately predicts the magnitude of the Southern Ocean decadal variability, we scatter Southern Ocean regional-mean SD against the ratios of $|\tilde{\eta}|/C$ to

$1-a$. We find that Eq. (4) works almost perfectly (Fig. 2A). This indicates decadal SAT variability can be indeed modeled as a linearly damped response to white-noise forcing from the atmosphere. The only exception to this is CNRM CM3, where the decadal variance of T' is much less than that predicted by the stochastic model. This suggests linear stochastic theory is not adequate to explain the Southern Ocean decadal variability in this simulation. Preliminary results show that this simulation exhibits a distinctive oscillation on multi-decadal to centennial time scales in the Southern Ocean. Physical processes responsible for this oscillation and its relevance to observed Southern Ocean's climate trends are currently under investigation.

5. Sources of Intermodel Spread

Since the magnitude of Southern Ocean decadal variability scales nearly perfectly with the ratio $|\tilde{\eta}|/C$ to $1-a$, we next assess relative contributions of $|\tilde{\eta}|/C$ and $1-a$ to the intermodel spread of the ratio of $|\tilde{\eta}|/C$ to $1-a$. To facilitate this, we take the logarithm of the ratio,

$$log(\frac{|\tilde{\eta}|/C}{1-a}) = log(|\tilde{\eta}|/C) - log(1-a) \tag{5}$$

From Eq. (5), we obtain an expression governing intermodel variance of decadal variability,

$$\begin{aligned} \sum[(log(\frac{|\tilde{\eta}|/C}{1-a}))']^2 = & \sum \; [(log(|\tilde{\eta}|/C))']^2 + \sum[(log(1-a))']^2 \\ - & \; 2\sum(log(|\tilde{\eta}|/C))'(log(1-a))' \end{aligned} \tag{6}$$

where $\sum$ represents the sum over all the simulations. The three terms on the right represent contributions of $log(|\tilde{\eta}|/C)$, $log(1-a)$ and their covariance.

These contributions, quantified as a percentage of the total variance (the term on the left side of Eq. (6)), are shown in Fig. 2B. We find the contribution of the covariance term to the intermodel variance of Southern Ocean decadal variability is negligible (white bar). The contribution of $log(1-a)$ (black bar) is about twice as large as the contribution of $log(|\tilde{\eta}|/C)$ (gray bar). This is consistent with the fact that the intermodel spread of a is much larger than that of $|\tilde{\eta}|/C$, as demonstrated in Section 4.

It is not straightforward to interpret this result physically, because C, the effective heat capacity, appears in both terms. If we rewrite $log(1-a)$ and $log(|\tilde{\eta}|/C)$ as

$$log(1-a) = log\lambda - logC + log\triangle t \tag{7}$$

$$log(|\tilde{\eta}|/C) = log|\tilde{\eta}| - logC \tag{8}$$

Eq. (5) then becomes

$$log(\frac{|\tilde{\eta}|/C}{1-a}) = log|\tilde{\eta}| - log\lambda - log\triangle t \tag{9}$$

Though $logC$ appears in Eqs. (7) and (8), it does not appear in Eq. (9). This suggests that decadal variability is determined by $|\tilde{\eta}|$ and λ only ($log\triangle t$ is of course the same for all models). The fact that C does not affect decadal variability can be also seen by plugging $a = 1 - \triangle t \cdot (\lambda/C)$ into Eq. (4). The physical interpretation for this is that the temperature anomalies are roughly in thermodynamic equilibrium with the forcing on decadal time scale. This is equivalent to the statement that the characteristic variability time scales of the models, C/λ are somewhat shorter than the decadal time scale, and that the first term on the left side of Eq. (1) for decadal temperature anomalies is negligible compared to the first term on the right side.

Since C does not affect decadal variability, variations in C do not contribute to intermodel spread of Southern Ocean decadal variability either. To the extent that variations in $logC$ contribute to spread in $log(1-a)$ and $|\tilde{\eta}|/C$, this should be reflected in the covariance term of Eq. (6). However, Fig. 2B shows this term is very small. There is a chance this could occur as a result of highly correlated intermodel variations of $log\lambda$ and $log|\tilde{\eta}|$ being almost perfectly anti-correlated with variations in $logC$. However, such a highly fortuitous cancellation effect seems unlikely. A much simpler and more plausible explanation is that spread in $log(1-a)$ in Fig. 2B arises from spread in $log\lambda$, while spread in $|\tilde{\eta}|/C$ stems from spread in $log|\tilde{\eta}|$, and the covariance term is a reflection of the element $log(1-a)$ and $|\tilde{\eta}|/C$ have in common, namely $logC$. For this reason, we judge that the first two columns of Fig. 2B represent contributions of variations in damping processes and AWNF to Southern Ocean decadal variability, and that damping processes dominate AWNF by roughly a factor of two.

We can also prove mathematically that $log\lambda$ makes a larger contribution to the spread in Southern Ocean decadal variability than $log|\tilde{\eta}|$. First, we obtain three expressions governing the intermodel variance of $log(1-a)$, $log(|\tilde{\eta}|/C)$ and $log(|\tilde{\eta}|/(C(1-a)))$ respectively, based on Eqs. (7)-(9). We then manipulate these expressions to obtain

$$\sum[(log\lambda)']^2 - \sum[(log|\tilde{\eta}|)']^2 = \sum[(log(1-a))']^2 - \sum[(log|\tilde{\eta}|/C)']^2 - 2\sum(log(\frac{|\tilde{\eta}|/C}{1-a})'(logC)' \tag{10}$$

The last term on the right side of Eq. (10) represents the covariance of $log(|\tilde{\eta}|/(C(1-a)))$ and $logC$. According to Eq. (9), $logC$ does not contribute to the intermodel spread of $log(|\tilde{\eta}|/(C(1-a)))$, so this term vanishes. Since the first term on the right side is 2 times larger than the second term, the right-hand side is positive. Therefore, $\sum[(log\lambda)']^2 > \sum[(log|\tilde{\eta}|)']^2$, indicating $log\lambda$ rather than $log|\tilde{\eta}|$ is the dominant cause of the intermodel spread of Southern Ocean decadal variability.

The effectiveness of damping processes, represented by λ, is largely determined by the strength of climate feedbacks involving surface albedo, cloud and water vapor. Thus intermodel differences in λ may stem largely from differing simulations of these feedbacks in the models. In contrast, atmospheric synoptic variability, whose impacts over the Southern Ocean are represented by $|\tilde{\eta}|$, may be more consistently simulated. These results suggest that efforts to improve climate simulations of Southern Ocean decadal variability ought to focus on processes affecting damping of temperature anomalies, including climate feedbacks. We note that these same feedbacks probably also shape the region's response to anthropogenic forcing. These efforts are necessarily long-term, involving more than one model development cycle. In the meantime, we may be able to constrain the lag-one autocorrelation a, a parameter probably mostly determined by λ. Values of a may be evaluated in paleoclimate records at coastal Antarctic locations whose decadal variability is linked to that of the surrounding ocean. This exercise may provide a much-needed observational constraint on the Southern Ocean's internal climate variability. We will describe this study in a forthcoming paper.

Acknowledgments.

This work was supported by NSF-0735056. We acknowledge the modeling groups, the Program for Climate Model Diagnosis and Intercomparison (PCMDI) and the WCRP's Working Group on Coupled Modelling (WGCM) for their roles in making available the

WCRP CMIP3 multi-model dataset. Support of this dataset is provided by the Office of Science, U.S. Department of Energy.

References

Cavalieri, D. J., P. Gloersen, C. L. Parkinson, J. C. Comiso and H. J. Zwally, 1997: Observed Hemispheric Asymmetry in Global Sea Ice Changes. *Science*, **278**(5340), 1104–1106.

Cavalieri, D. J. and C. L. Parkinson, 2008: Antarctic sea ice variability and trends, 1979-2006. *J. Geophys. Res.*, **113**, C07004, doi:10.1029/2007JC004564.

Hall, A., 2004: The role of surface albedo feedback in climate. *J. Climate*, **17**, 1550–1568.

Hall, A. and S. Manabe, 1997: Can local linear stochastic theory explain sea surface temperature and salinity variability. *Climate Dyn.*, **13**, 167–180.

Hasselmann, K., 1976: Stochastic climate models. Part I: Theory. *Tellus*, **28**, 473–485.

Lemke, P., E. W. Trinkl and K. Hasselmann, 1980: Stochastic dynamics analysis of polar sea ice variability. *J. Phys. Oceanography.*, **10**, 2100–2120.

Liu, J. P., J. A. Curry and D. G. Martinson, 2003: Interpretation of recent Antarctica sea ice variability. *Geophys. Res. Lett.*, **31**, L02205, doi:10.1029/2003GL018732.

Manabe, S. and R. J. Stouffer, 1996: Low-frequency variability of surface air temperature in a 1000-year integration of a coupled atmosphere-ocean–land surface model. *J. Climate*, **9**, 376–393.

North, G. R., R. F. Cahalan and J. A. Coakley Jr., 1981: Energy Balance Climate Models. *Rev. Geophys. Space Phys.*, **19**(1), 91–121.

Parkinson, C. L. and D. J. Cavalieri, 2008: Arctic sea ice variability and trends, 1979-2006. *J. Geophys. Res.*, **113**, C07003, doi:10.1029/2007JC004558.

Rothrock, D. A., Y. Yu and G. A. Maykut, 1999: Thinning of the Arctic Sea-ice Cover. *Geophys. Res. Lett.*, **26**(23), 3469–3472.

Serreze, M. C., J. A. Maslanik, T. A. Scambos, F. Fetterer, J. Stroeve, K. Knowles, C. Fowler, S. Drobot, R. G. Barry and T. M. Haran, 2003: A record minimum Arctic sea ice extent and area in 2002. *Geophys. Res. Lett.*, **30**(3), 1110, doi:10.1029/2002GL016406.

Stroeve, J., M. Serreze, S. Drobot, S. Gearheard, M. Holland, J. Maslanik, W. Meier and T. Scambos, 2008: Arctic sea ice extent plummets in 2007. *Eos Trans. AGU*, **89**(2), doi:10.1029/2008EO020001.

Vaughan, D. G., G. J. Marshall, W. M. Connolley, C. Parkinson, R. Mulvaney, D. A. Hodgson, J. C. King, C. J. Pudsey and J. Turner, 2003: Recent rapid regional climate warming on the Antarctic Peninsula. *Clim. Change*, **60**, 243–274, doi:10.1023/A:1026021217991.

Vinnikov, K. Y., A. Robock, R. J. Stouffer, J. E. Walsh, C. L. Parkinson, D. J. Cavalieri, J. F. B. Mitchell, D. Garrett and V. F. Zakharov, 1999: Global warming and northern hemisphere sea ice extent. *Science*, **286**, 1934–1937.

Williams, A. B. and F. J. Taylor, 1988: Electronic Filter Design Handbook: LC, Active, and Digital filter. *2th Edition,* McGraw-Hill Publishing Company.

Figure Captions

Figure 1: Zonal-mean standard deviation (SD) of (A) annual-mean surface air temperature (SAT), (B) annual-mean sea-ice cover (SIC), (C) decadal SAT and (D) decadal SIC in the SH extratropics. An order 2 lowpass Chebyshev filter is used to obtain decadal SAT and SIC time series [Williams and Taylor, 1988]. SD of the quantities is calculated at each grid point and then averaged zonally to get the zonal-mean. Gray lines in each panel represent individual simulations and thick black lines the ensemble-means.

Figure 2: A. Scatterplot of regional-mean SD of decadal SAT over the Southern Ocean against $|\tilde{\eta}|/(C(1-a))$. B. Percentages of intermodel variance of $log(|\tilde{\eta}|/(C(1-a)))$ of SAT that can be attributed to intermodel variations of $log(1-a)$ (black bar), $log(|\tilde{\eta}|/C)$ (gray bar) and their covariance (white bar). See the text for details on these calculations.

Table 1. 15 AR4 climate models used in this study and associated regional-mean values of various quantities over the Southern Ocean: (3rd column) SD of decadal SAT, and (4th column) SD of decadal SIC. It is calculated at each grid point and then averaged over the Southern Ocean to get the regional-mean. (5th column) lag-one year autocorrelation coefficient, a of annual-mean SAT. It is calculated at each grid point and then averaged over the Southern Ocean to get the regional-mean. (6th column) $|\tilde{\eta}|/C$ of SAT. See text for details on these calculations. Oceanic regions south of 50^0S are used in the regional-mean calculations for SAT, and sea-ice covered areas in the Southern Ocean are used in the regional-mean calculations for SIC. These areas are also used in the subsequent regional-mean calculations. Note that SIC of ECHAM5/MPI-OM and ECHO-G were not available when the analysis was performed, indicated by "NA".

No.	model	SAT SD (K)	SIC SD (%)	a	$\lvert\tilde{\eta}\rvert/C$ (Kyear$^{1/2}$)
1	CCSM3	0.31	2.39	0.13	0.80
2	CGCM3.1(T47)	0.40	2.19	0.25	1.00
3	CGCM3.1(T63)	0.43	2.19	0.13	1.18
4	CNRM-CM3	0.61	4.07	0.65	0.86
5	CSIRO Mk3.5	0.37	2.79	0.29	0.88
6	ECHAM5/MPI-OM	0.43	NA	0.32	0.94
7	ECHO-G	0.53	NA	0.47	0.95
8	GFDL CM2.0	0.51	3.00	0.43	0.96
9	GFDL CM2.1	0.36	2.46	0.33	0.78
10	GISS-ER	0.25	2.26	0.30	0.62
11	IPSL CM4	0.37	3.09	0.30	0.80
12	MIROC3.2(medres)	0.35	2.69	0.44	0.64
13	MRI CGCM2.3.2	0.35	2.95	0.30	0.76
14	PCM	0.45	3.27	0.37	0.90
15	UKMO HadCM3	0.35	2.24	0.20	0.88

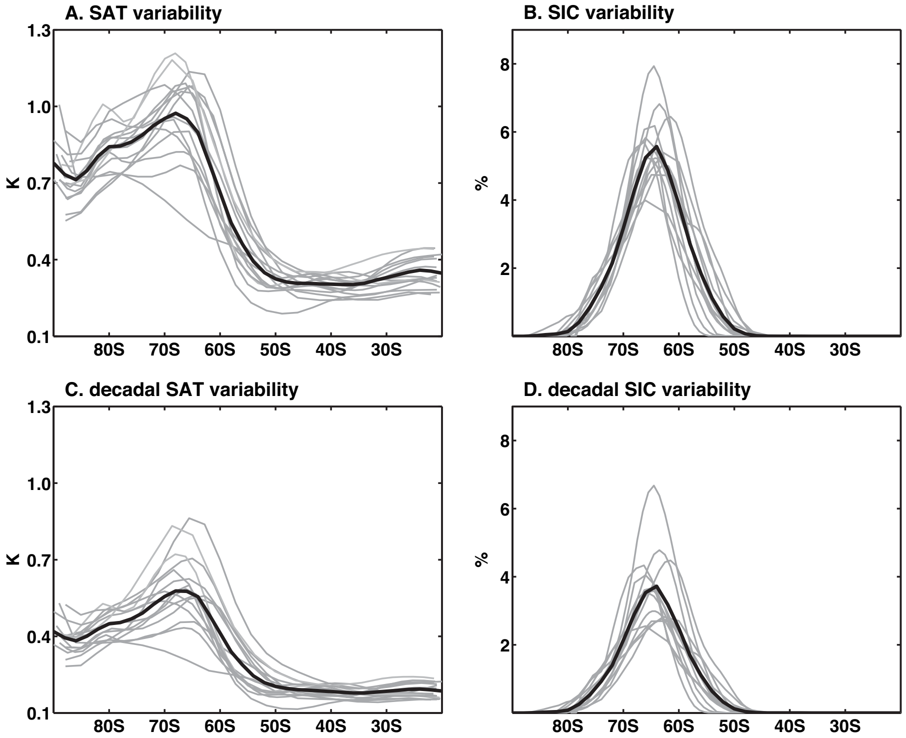
A. SAT variability
K
1.3
1.0
0.7
0.4
0.1
80S
70S
60S
50S
40S
30S
B. SIC variability
%
8
6
4
2
80S
70S
60S
50S
40S
30S
C. decadal SAT variability
K
1.3
1.0
0.7
0.4
0.1
80S
70S
60S
50S
40S
30S
D. decadal SIC variability
%
8
6
4
2
80S
70S
60S
50S
40S
30S

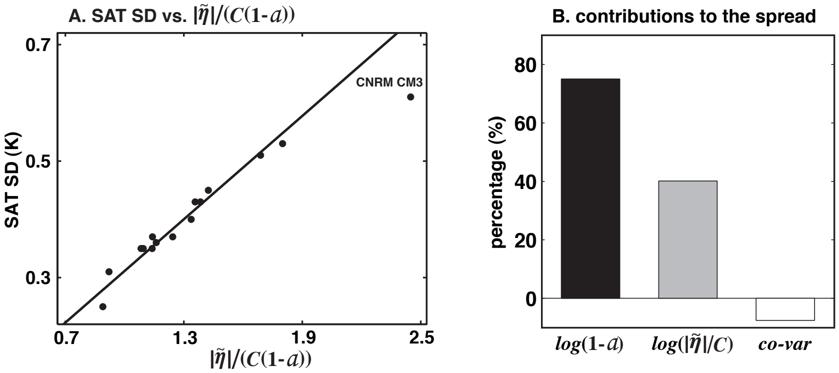
A. SAT SD vs. $|\tilde{\eta}|/(C(1-a))$
SAT SD (K)
0.7
0.5
0.3
0.7
1.3
1.9
2.5
$|\tilde{\eta}|/(C(1-a))$
CNRM CM3
B. contributions to the spread
percentage (%)
80
60
40
20
0
$log(1-a)$
$log(|\tilde{\eta}|/C)$
co-var